Soil Moisture–Atmosphere Interaction in a Moist Semigeostrophic Model of Baroclinic Instability

FABIO CASTELLI

Istituto di Idraulica, Università degli Studi di Perugia, Perugia, Italy

IGNACIO RODRIGUEZ-ITURBE

Department of Civil Engineering, Texas A&M University, College Station, Texas

15 July 1994 and 1 December 1994

ABSTRACT

Attention is focused on the dynamical coupling between the soil moisture and atmospheric processes, such as in the presence of a growing moist baroclinic wave. A simplified scheme, representing the mass and energy exchanges between the soil and the atmospheric boundary layer, is incorporated into the inviscid semigeostrophic equations for the evolution of a meridionally independent baroclinic disturbance in the moist atmosphere. The model is formulated in terms of coupled, nonlinear, ordinary differential equations, allowing for simple and extensive numerical simulations. Using such an approach, the question is addressed to what extent and through which mechanisms a heterogeneous soil moisture distribution affects the evolution of the baroclinic waves and in particular the estimate of the potential precipitation. The interaction between land and atmosphere is found to have both a local effect and a large-scale effect. The local effect consists of modifying the vertical lapse rates of dry and equivalent potential temperatures in the troposphere. The large-scale effect is realized through the global dynamics of the baroclinic wave and in particular through the rates of mass and energy advection and the strength of the ageostrophic frontal circulation, which depend strongly themselves on the temperature lapse rates. Both mechanisms are found to be substantially dependent on both the local moisture content of the soil and on the large-scale moisture differences, highlighting their feedback on precipitation.

1. Introduction

Some recent works, based on simulations of case studies with primitive equation numerical models, have addressed the possible effects of heterogeneous soil moisture distributions on large mesoscale circulation. In Chang and Wetzel (1991), the prestorm environment connected to the development of a convective complex in Nebraska on 3–4 June 1980 was analyzed by comparing different simulations based on different hypotheses on the soil moisture and vegetation distributions; spatial variations in both quantities were found to lead to the enhancement of a stationary front. With a similar approach, Fast and McCorcle (1991) analyzed the passage of a summer cold front in the central United States. The evaporating heterogeneous soil was found to significantly alter the structure of the boundary layer embedded in the baroclinic circulation. As a result, the front was then weakened near the surface, with an increase of moisture convergence in several locations and the advection of the evaporated moisture far from the origin. Both studies recognized the important role of soil moisture in modifying the spatial distribution and intensity of precipitation, still highlighting a strong dependence of these effects on the particular synoptic conditions.

Other studies, such as Ookouchi et al. (1984) and Segal et al. (1988), already indicated that the intensity of thermal circulation induced by soil heterogeneity may reach, even in the absence of significant synoptic forcing, that of sea-breeze circulation.

Taking these results as "evidence" of significant effects of soil moisture on precipitation at a variety of scales, there is a need for a deeper conceptual understanding of the underlying feedback mechanisms.

We may ask, as a first question, if there exists a preferred coupling between the alternation of warm–cold anomalies of a baroclinic circulation and large-scale spatial patterns in the soil moisture distribution. By preferred we mean that given uniform initial conditions in all the variables other than the soil moisture distribution the coupling could lead either to a faster growth of the corresponding wave or, more importantly, to a higher estimate of the precipitation produced in the cyclonic areas.

The effect of a "moist" surface boundary on the development of ideal baroclinic waves was studied in

Corresponding author address: Dr. Fabio Castelli, Istituto di Idraulica, Università degli Studi di Perugia, Facoltà di Ingegneria, Loc. S. Lucia, 6125 Perugia, Italy.

Fantini (1991), for example. Such a study was based on the two-level moist semigeostrophic model of Emanuel et al. (1987, E87 hereafter), with the addition of parameterized heat and moisture fluxes from a warm sea body. In a qualitative way, given the simplified form of the model and the restriction of the "warm sea" case (evaporation always present at its potential rate), the study clarified some important mechanisms leading to an increase—with respect to the "no fluxes" solutions—of the growth rate and phase speed of unstable baroclinic waves.

We will then proceed along a similar line; that is, we will first include a simplified scheme of soil–atmosphere interaction in the E87 model and then discuss the results from an extended set of solutions, where a variety of hypotheses on the soil moisture availability are made.

2. Formulation of the model

We consider the inviscid semigeostrophic model of moist baroclinic instability of E87, describing the growth of Y-independent periodic perturbations in the semigeostrophic $(X, Z) \in (-\infty, +\infty) \times (0, 2H)$ plane, forced by a uniform zonal shear $U_g = U_z(Z - H)$.

Defining a reference value for the zonal velocity as $U = U_z H/2$ and the nondimensional vertical stability parameter $\alpha = HQ_0/g$, where Q_0 is the Ertel's dry potential vorticity for the undisturbed base state, nondimensional variables (lower case) are defined as in Table 1.

Then the various equations that rule the free-atmosphere dynamics become

$$\frac{\partial v}{\partial z} = \frac{\partial \theta}{\partial x}, \tag{1}$$

$$\frac{\partial v}{\partial t} + 2z\frac{\partial v}{\partial x} = \frac{\partial \psi}{\partial z}, \tag{2}$$

$$\frac{\partial \theta}{\partial t} + 2z\frac{\partial \theta}{\partial x} + q^*\frac{\partial \psi}{\partial x} = 2v, \tag{3}$$

$$\frac{\partial \theta_e}{\partial t} + 2z\frac{\partial \theta_e}{\partial x} + q_e\frac{\partial \psi}{\partial x} = 2(\Gamma_d/\Gamma_m)v, \tag{4}$$

$$\frac{dq}{dt} = \xi\frac{\partial}{\partial z}\frac{d\theta}{dt}, \tag{5}$$

$$\frac{dq_e}{dt} = \xi\frac{\partial}{\partial z}\frac{d\theta_e}{dt}, \tag{6}$$

where

$$\xi = \frac{1}{1 - \dfrac{\partial v}{\partial x}}, \tag{7}$$

TABLE 1. Definitions, scaling relations, and orders of magnitude (dimensional value corresponding to one nondimensional unit) for main variables used in the model. The orders of magnitude are estimated according to the parameter values reported in section 3.

Variable	Scaling	Magnitude
Zonal coordinate	$X = [(HQ_0^{1/2})/f]x$	5.83×10^5 m
Vertical pressure coordinate	$Z = Hz + H$	5×10^3 m
Time	$T = [(HQ_0^{1/2})/(fU)]t$	3.89×10^4 s
Dry potential vorticity	$Q = Q_0 q$	1.36×10^4 s^{-2}
Moist potential vorticity	$Q_e = Q_0 q_e$	1.36×10^{-4} s^{-2}
Absolute vorticity (vertical component)	$\Xi = f\xi$	10^{-4} s^{-1}
Ageostrophic streamfunction	$\Psi = HU\psi$	7.50×10^4 m^2 s^{-1}
Potential temperature anomaly (log)	$\ln\Theta = \alpha\theta + \ln(\Theta_0)$	6.93×10^{-2}
Equivalent potential temperature anomaly (log)	$\ln\Theta_e = \alpha\theta_e + \ln(\Theta_0)$	6.93×10^{-2}
Soil slab absolute temperature	$T_s = \Theta_0\tau_s$	280 K
Zonal geostrophic velocity	$U_g = 2Uz$	30.0 m s^{-1}
Meridional geostrophic velocity	$V_g = HQ_0^{1/2}v$	58.3 m s^{-1}

$$q^* = \begin{cases} q = \xi\dfrac{\partial \theta}{\partial z}; & \text{unsaturated downdraft} \\ \dfrac{\Gamma_m}{\Gamma_d}q_e = \dfrac{\Gamma_m}{\Gamma_d}\xi\dfrac{\partial \theta_e}{\partial z}; & \text{saturated updraft.} \end{cases} \tag{8}$$

The last definition, where Γ_m and Γ_d are the moist and dry ambient lapse rates, takes into account the latent heat release due to vapor condensation. As analyzed in E87, the dynamics of the baroclinic wave is strongly dependent on the values of q and q_e, the second being much smaller than the first in a saturated atmosphere.

Our interest is in analyzing the possible impacts of soil moisture–atmosphere interaction on such dynamics. We will then modify the above-outlined E87 model, and in particular the forcing terms of Eqs. (5) and (6), in order to take into account, in a simplified framework, the sensible and latent heat exchange between an ideal uniform soil, with heterogeneous moisture distribution, and the atmosphere.

To this purpose, we consider a well-mixed atmospheric boundary layer of thickness $z^* \ll H$ and define inside of this region vertical-averaged values θ_b and θ_{eb} of the potential and equivalent potential temperatures. A variety of parameterizations, which rely on the accurate estimation of the soil response to solar radiation and hence the diurnal cycle, have been proposed in the literature for the thickness of the atmospheric boundary layer. The model used here is far below such a level of detail, in particular with respect to the representation of the atmospheric and soil vertical profiles. We also stress again that we are investigating the possible feed-

backs of soil moisture on large-scale dynamics, such as cyclonic convergence, rather than on small-scale deep convection. Therefore, we are interested in the boundary layer dynamics only as a "filter" between the soil and the troposphere, with no direct role in the precipitation occurrence. Finally, we note that in the numerical simulations of Fast and McCorcle (1991) the variability on the soil moisture distribution was found to have a significant effect on the average temperature and humidity of the boundary layer but a much less relevant effect on its thickness. On the basis of these considerations, we are assuming the approximation of a constant boundary layer thickness z^*.

At the same level of approximation, we consider a "surface" soil slab of constant depth Z_r, where we define the vertically averaged saturation ratio s, the absolute temperature τ_s, and the equivalent temperature at saturation $\tau_{es}(\tau_s)$.

Denoting with f_{Qh} and f_{QE} the nondimensional sensible and total heat fluxes from the soil and with r_n the net radiative flux into the soil, the soil–atmosphere interface thermodynamics is described by the heat balance equations of the two air and soil slabs:

$$\frac{d\theta_b}{dt} = b_a f_{Qh} \exp(-\alpha\theta_b), \tag{9}$$

$$\frac{d\theta_{eb}}{dt} = b_a f_{QE} \exp(-\alpha\theta_{eb}), \tag{10}$$

$$\frac{d\tau_s}{dt} = b_s(r_n - f_{QE}), \tag{11}$$

where

$$r_n = n_r(1 - \tau_s^4), \tag{12}$$

$$f_{Qh} = \tau_s - \exp(\alpha\theta_b), \tag{13}$$

and the constants b_a, b_s, and n_r are defined as

$$b_a = \frac{k^2 g}{z^* f Q_0^{1/2}} \left[\frac{U^*}{U \ln^2(z^*/z_0)}\right], \tag{14}$$

$$b_s = \left(\frac{\rho_b C_p z^*}{\rho_s C_s Z_r}\right) \alpha b_a, \tag{15}$$

$$n_r = \epsilon \frac{\sigma \Theta_0^3}{k^2 \rho_b C_p U} \left[\frac{U^*}{U \ln^2(z^*/z_0)}\right]^{-1}. \tag{16}$$

Here k is the von Kármán constant, ρ_s and C_s are representative values of the soil density and specific heat, σ is the Stefan–Boltzman constant, and ϵ is a factor smaller than 1. The quantity r_n in Eq. (12) represents the contribution to the radiative balance of temperature changes in the soil, under the hypothesis of an initial equilibrium. The actual total heat flux f_{QE} will be a function of soil saturation s and the potential total heat flux $f_{QE\text{pot}}$, whose expression is now

$$f_{QE\text{pot}} = \tau_{es} - \exp(\alpha\theta_{eb}). \tag{17}$$

If we denote with R the ratio between the sensible and the potential latent heat fluxes from the soil (analogous to a potential Bowen ratio), we have

$$f_{QE} = \left[1 + \frac{G^*(s)}{R}\right] f_{Qh}, \tag{18}$$

or alternatively

$$f_{QE} = \left[\frac{G^*(s) + R}{1 + R}\right] f_{QE\text{pot}}, \tag{19}$$

where $G^*(s)$ represents the role of soil saturation in partitioning the total flux into sensible and latent. We will represent it as a monotone polynomial form (Lowry 1959), increasing with s when $f_{QE\text{pot}}$ is positive, and decreasing in the opposite case. The assumption of having a soil moisture dependence also for the condensation process (negative $f_{QE\text{pot}}$) is based on neglecting the condensation on the soil and vegetation surfaces with respect to the condensation occurring inside the soil pores. A quantification of the relevance of the surface condensation with respect to the "inside soil" condensation would require a much more detailed type of modeling, taking explicitly into account the air and vapor fluxes inside the soil pores. Our main concern, however, is to include the heat fluxes in a "bulk" thermodynamic balance of the soil and atmospheric slabs. We speculate that the surface condensation is prevented by the well-developed turbulence inside the atmospheric boundary layer in the presence of a strong wind shear. On the basis of this reasoning, we have implicitly assumed that, in terms of net heat exchange between the soil and the atmospheric slabs, inside soil saturation is more relevant than dewfall for the specific "weather condition" we are considering in our study.

Many of the essential features of the just formulated model can be captured with a crude discretization of a two-dimensional flow domain. In particular, we consider the evolution of a y-independent baroclinic wave, whose half-wavelength L is considered a parameter. We then define representative values of the various quantities at appropriate levels, averaged horizontally over a length L. We assume that a single period of the flow domain can be subdivided into a region 1 where the vertical velocity is downward corresponding to the cold anomaly of the perturbation and a region 2 of saturated updraft in the warm anomaly, both of length L (Fig. 1). In doing this, we are neglecting the contraction of the updraft region, with respect to the downdraft, due to the difference between the values of the dry and the equivalent potential vorticities. However this effect is relevant, as shown in E87, when the equivalent potential vorticity in the updraft region is much smaller than the dry one in the downdraft. This difference will be, as shown later, strongly reduced by the soil interaction, which has a stabilizing effect on the moist vertical profile in the warm anomaly and a destabilizing effect in the cold anomaly.

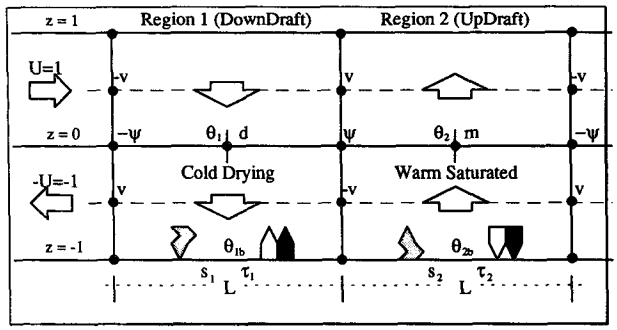

FIG. 1. Structure of the discretized model domain for a baroclinic wave of period $2L$.

Going back to the definition of our simplified model, the vertical representation of the flow domain is based on a two-layer discretization (Fig. 1). Fixed values $U = \pm 1$ of the zonal velocity are prescribed in the center of each layer ($z = \pm 1/2$), while four representative values of the perturbation meridional velocity v are defined at the same levels at the interfaces between region 1 and region 2. It is easy to show that four such velocities have the same absolute value, changing sign in a chessboard-like fashion. Two nontrivial values of the ageostrophic streamfunction are defined at the cross points between the vertical layers and region interfaces ($z = 0$), again found to have the same absolute value and opposite sign. We assume the convention that v and ψ are positive at the interface where the downdraft is on the left (with positive v in the upper layer). We also define average values of the free-atmosphere potential temperature θ_1 and θ_2 at the midlevel ($z = 0$) inside each region. Representative values of the dry potential vorticity d for the downdraft region and of the equivalent potential vorticity m for the updraft region are also defined at the midlevel. Finally, the soil–atmosphere interface state (at $z = -1$)—averaged inside each region—is represented by the values θ_{b1} and θ_{eb2} of the boundary layer potential (equivalent in region 2) temperatures, τ_1 and τ_2 of the soil absolute temperatures, and s_1 and s_2 of the soil saturation.

Using finite differencing for the spatial derivatives, upwind in the horizontal according to the sign of U, and upwind averaging for the forcing term in the thermodynamic equation, the following set of coupled ordinary differential equations is finally obtained (the overdot stands for time derivative):

$$\dot{v} = -\frac{2}{L}v - \psi, \tag{20}$$

$$\dot{\theta}_1 = -2v - \frac{2}{L}d\psi, \tag{21}$$

$$\dot{\theta}_2 = 2v + \frac{2}{L}m\psi, \tag{22}$$

$$\dot{\tau}_1 = b_s\left\langle n_r(1-\tau_1^4) - \left[1 + \frac{G^*(s_1)}{R}\right] \times \left\{\tau_1 - \exp\left[\alpha\left(\theta_1 - \frac{L+2v}{L}d\right)\right]\right\}\right\rangle, \tag{23}$$

$$\dot{\tau}_2 = b_s\left\langle n_r(1-\tau_2^4) - \left[\frac{G^*(s_2)+R}{1+R}\right]\left\{\tau_{e2\text{sat}}(\tau_2) - \exp\left[\alpha\left(\theta_{e2\text{sat}}(\theta_2) - \frac{\Gamma_d(L-2v)}{\Gamma_m L}m\right)\right]\right\}\right\rangle, \tag{24}$$

$$\dot{d} = -b_a\left\{\tau_1 - \exp\left[\alpha\left(\theta_1 - \frac{L+2v}{L}d\right)\right]\right\} \times \exp(-\alpha\theta_{b1}), \tag{25}$$

$$\dot{m} = -\frac{\Gamma_m}{\Gamma_d}b_a\left[\frac{G^*(s_2)+R}{1+R}\right]\left\{\tau_{e2\text{sat}}(\tau_2) - \exp\left[\alpha\left(\theta_{e2\text{sat}}(\theta_2) - \frac{\Gamma_d(L-2v)}{\Gamma_m L}m\right)\right]\right\} \times \exp(-\alpha\theta_{eb2}), \tag{26}$$

where the definition of the potential vorticities has been used to estimate the boundary layer temperatures and the streamfunction is diagnosed from the equation

$$\psi = -\frac{4Lv}{L^2 + d + m}. \tag{27}$$

As in E87, an initially saturated atmosphere is assumed for a convenient mathematical formulation of the instability problem. Nevertheless, such an assumption may be too crude for the dynamics of a baroclinic cold anomaly, like the one region 1 must represent. In particular, the boundary layer vapor deficit due to the simple downdraft drying effect may be too small, in comparison with the usual observed values in the real atmosphere under clear-sky conditions, for a correct estimation of the latent heat fluxes (evaporation) from the soil. For this reason, we assume the potential Bowen ratio as a known parameter and calculate the potential total flux on the basis of it. The actual total flux is then calculated taking into account the soil saturation. In this way, we obtain both the congruence with the definition of an initial equilibrium condition and a more reasonable estimate of the evaporation flux, still highly dependent on the soil saturation. A similar reasoning is applied to region 2.

We observe that substitution of the relation (27) into (20) leads to the homogeneous equation

$$\dot{v} = \sigma v, \tag{28}$$

where

$$\sigma = \frac{2}{L}\left[\frac{L^2 - (d+m)}{L^2 + (d+m)}\right]. \tag{29}$$

The initial growing stage of the baroclinic perturbation can be studied analytically by linearization of the above equation, that is, by neglecting the variations in time of m and d. In this case, σ is time independent and the equation has the general nontrivial solution $v = v_0 \exp(\sigma T)$, with a short-wave cutoff at $L = (d + m)^{1/2}$ and a maximum initial growing rate $\sigma_{\max} = 0.6006\,(d + m)^{-1/2}$ at $L = 2.058\,(d + m)^{1/2}$. Beyond the initial linear stage, variations of d and m may become relevant because of the interaction with the soil, so that the growth rate and, as a consequence, the circulation at the time of the eventual frontal collapse will be affected as well.

As the baroclinic perturbation grows, we expect a reduction of the ambient vertical lapse rate (hence of d) in region 1 because of the heat flux from a soil that will tend to be warmer than the developing atmospheric cold anomaly. The opposite is expected in region 2 (increasing of m). Because of evaporation of the soil moisture, the heat flux in region 1 will be "partitioned" according to the particular soil saturation into sensible and latent, but only the sensible one will be "used" in reducing the dry potential vorticity d. Then the soil saturation distribution, in controlling such a partitioning, will have a prominent role in how differently d and m evolve over time and, hence, in the dynamics of the perturbation growth up to the frontal collapse.

3. Numerical simulations

The numerical simulations we are going to describe have been performed with the above-described model and taking the following values for the various atmospheric and climatic parameters: $\Theta_0 = 280$ K; $Q_0 = 1.36 \times 10^{-4}$ s^{-2}; $f = 10^{-4}$ s^{-1}; $U = 15$ m s^{-1}; $H = 5 \times 10^3$ m; $k = 0.4$; $g = 9.81$ m s^{-2}; $C_p\rho_b = 2.28 \times 10^3$ J m^{-3} K^{-1}. The soil is characterized by the reference thermal capacity $C_s\rho_s = 10^6$ J m^{-3} K^{-1}. Derived scales for the various quantities are reported in Table 1. The following relations can be readily obtained from these values:

$$b_a = 1.35 \times 10^4 \left[\frac{U^*}{U \ln^2(z^*/z_0)}\right], \tag{30}$$

$$\frac{b_s}{b_a} = 1.5 \times 10^{-4} \frac{z^*}{Z_r}, \tag{31}$$

$$n_r = 2.18 \times 10^{-2}\, \epsilon \left[\frac{U^*}{U \ln^2(z^*/z_0)}\right]^{-1}. \tag{32}$$

At a boundary layer thickness z^* of about 100 m, the dimensionless group on the right-hand side of (30) may be, for various soil roughness, in the range 10^{-3}/10^{-2}. Also, with an "active" soil depth of a few centimeters, it is $b_s \approx b_a/10$. We then choose the set of parameters $(b_a, b_s, n_r) = (20, 2, 0.3)$ and a potential Bowen ratio $R = 0.3$.

The function $G^*(s)$, which will serve to calculate the actual evaporation rate starting from its potential value, is defined on the basis of the monotone function $\Gamma(s) = 2.8s - 2.6s^2 + 0.8s^3$ as

$$G^*(s) = \begin{cases} \Gamma(s); & f_{QE\text{pot}} \geq 0 \\ 1 - \Gamma(s); & f_{QE\text{pot}} < 0. \end{cases} \tag{33}$$

A first set of simulations has been performed considering four opposite and extreme soil moisture distributions, according to the following schemes:

D1W2: Totally dry soil in region 1 and totally wet soil in region 2. No possibility of either evaporation or condensation from/into the soil $[G^*(s_1) = G^*(s_2) = 0]$.

W1D2: Totally wet soil in region 1 and totally dry soil in region 2. Evaporation and condensation from/into the soil at their potential rate $[G^*(s_1) = G^*(s_2) = 1]$.

W1W2: Totally wet soil in both regions. Evaporation from the soil at its potential rate $[G^*(s_1) = 1]$ and no condensation into the soil $[G^*(s_2) = 0]$.

D1D2: Totally dry soil in both regions. Condensation into the soil at its potential rate $[G^*(s_2) = 1]$ and no evaporation from the soil $[G^*(s_1) = 0]$.

Keeping in mind that precipitation is going to occur in region 2, the main goal of these first simulations is to establish which one among the four extreme soil moisture distributions, is more "favorable" in terms of perturbation growth and rainfall production. In particular, the case of higher precipitation for the W2 cases (precipitation on wet soil) would indicate the existence of a positive feedback between soil moisture and precipitation. Furthermore, an overall higher precipitation for the D1W2 case would indicate a tendency to be spatially structured for such a feedback.

The simulations are started with a small perturbed value $v_0 = 0.001$, and then the system of Eqs. (20)–(26) is integrated numerically up to the time when the value of $\xi_{\max} = 100$ in the low-level vorticity is approximately reached, marking the occurrence of the frontal collapse.

Figure 2 shows the temporal evolution of the maximum low-level vorticity for the four different soil moisture distributions, with a semiperiod of the perturbation $L = 2.0$; the uniform W1W2 and D1D2 schemes show almost identical vorticity evolution. The D1W2 and W1D2 schemes are instead accelerated and slowed, respectively, with a difference of about 1.4 time units (about 11 hours, according to the chosen parameters) between them in reaching the same frontal collapse. As a first result, we have the growth of the baroclinic wave favored from a heterogeneous soil moisture distribution with wetter soil under the warm-precipitating anomaly.

The growth of the perturbation is strictly dependent on the quantity $(d + m)$, which may be considered a "global" stability parameter (sum of the dry stability in the cold anomaly and moist stability in the warm

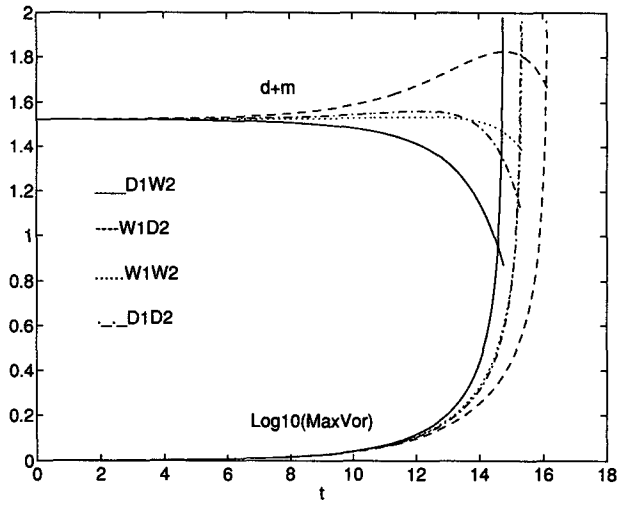

FIG. 2. Temporal evolution of the low-level maximum absolute vorticity $\xi_{max} = L/(L - 2v)$ and of the sum of the dry and equivalent potential vorticities $d + m$, for the four different soil moisture distributions (D1W2, W1D2, W1W2, D1D2) over the baroclinic wavelength $2L = 4.0$, up to the time when $\xi_{max} \approx 100$.

anomaly). The evolution of such a quantity, for the four schemes, is depicted again in Fig. 2. It is interesting to note that only in D1W2 is the stability evolution monotone and, in particular, monotonically decreasing. In this case, we then have an increasingly faster perturbation growth as it approaches the frontal collapse, with respect to the "no-soil" linear solution (constant d and m). In the end, the global stability is reduced by about 40%. In the three other schemes, the growth is slower at the middle stage of the evolution (increasing global stability) than the no-soil solution; such a middle-stage slowing is much stronger in the W1D2 case, which is when the warm-precipitating anomaly develops above the dry soil.

The effects of the heat partitioning played by the soil moisture are more evident looking at the time evolution of the various heat fluxes, depicted in Fig. 3. Starting with the analysis of the sensible heat flux from the soil of region 1, we observe that, as expected, the more evident difference is found between the schemes where the soil of region 1 is either dry (D1W2 and D1D2) or wet (W1W2 and W1D2). The soil tends to adjust to the colder air temperatures by releasing sensible and, when soil moisture is available, latent heat. Such a response to the atmospheric forcing is then partitioned in very different ways. In the D1 schemes all the fluxes from the soil in region 1 have to be in the form of sensible heat, while 70% of the fluxes from the saturated W1 soil are in the form of latent heat, so that the sensible heat flux is strongly reduced. Also the total heat flux evolution is very different in region 1. In reducing its vertical stability because of the heat fluxes from the soil, the atmosphere tends to adjust to the warmer soil temperature, but only the sensible part is "used" to this purpose in region 1. If all the flux is in the form of sensible heat, the mutual "adjusting" process is much more efficient, and less total heat exchange is required.

Quite different is the picture in region 2. Here, we have hypothesized a saturated thermodynamics for the growing warm moist anomaly. The driving mechanism for the heat exchange is then the difference between the equivalent air temperature and the saturation soil temperature. All the heat flux (sensible and latent), now directed by the warming air into the soil, is used in the mutual-adjusting process. In other words, now that the total heat flux is the main concern, and not the sensible only as in region 1, the partitioning of the heat played by the soil moisture is much less relevant. The difference between the total heat fluxes in region 2 of the W2 and D2 schemes is much less than the difference between the total heat fluxes in region 1 of the W1 and D1 schemes.

Going back to the primary goal of these simulations, which is an estimate of the "rainfall potential," we may suppose that such a potential is proportionally related to the vertical velocity $w = 2\psi/L$ and inversely related to the vertical moist stability—here represented by the midlevel equivalent potential vorticity m. The evolution of two such quantities is represented in Fig. 4. We expect the vertical velocity to be stronger for smaller global stability ($d + m$) and equal to the level of evolution of the baroclinic wave (equal value of v). The D1W2 scheme shows the strongest and fastest evolving vertical velocity among the four, while the opposite occurs with W1D2. Furthermore, the vertical moist stability m in the same region is progressively increased more in D2 schemes than in W2 ones. Clas-

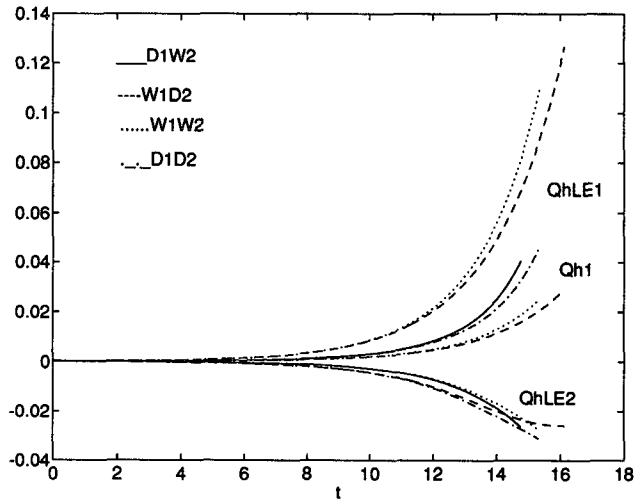

FIG. 3. As in Fig. 2 but for the fluxes f_{Qh1} and f_{QE1} of sensible and total heat released from the soil underlying the cold anomaly and for the total flux f_{QE2} released from the soil underlying the warm anomaly. The fluxes f_{Qh1} and f_{QE1} are equal for the soil moisture distributions D1D2 and D1W2.

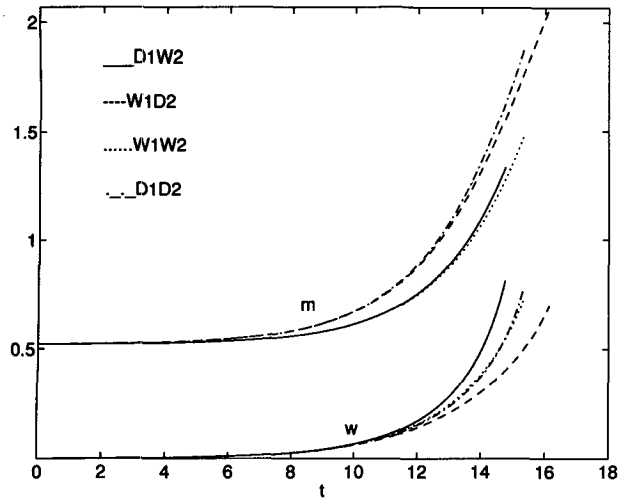

FIG. 4. As in Fig. 2 but for the equivalent potential vorticity m and the midlevel vertical velocity w in the warm anomaly.

sifying finally the four schemes in terms of rainfall potential, D1W2 is the most favorable (high W and low m), W1W2 is second (medium W and low m), D1D2 is third (medium W and high m), and W1D2 is the least favorable (low W and high m).

Once we have established the fundamental underlying dynamics and through which mechanisms this is controlled by the soil moisture distribution, we may move to a more synthetic type of study. To have a more complete picture of the sensitivity of the problem on the spatial distribution of soil moisture, a more extensive second series of simulations has been performed varying both the perturbation wavelength L and the average soil saturation in the two regions. In particular, we will consider soil moisture distributions such that $\Gamma(s_1) + \Gamma(s_2) = 1$ and analyze the solutions in terms of final growing rate and rainfall potential near the frontal collapse for different wavelengths L and values of the difference $\Gamma(s_2) - \Gamma(s_1)$ in the range $[-1, 1]$. In doing this, we take as representative of the final growing rate the inverse of the last doubling time of the perturbation amplitude (time span occurred to evolve from $v = L/4$ to $v = L/2$). The rainfall potential is instead represented by an ad hoc precipitation index R that, given the increasing moist stability toward positive finite values, is simply defined as $R = W/m$. This may be considered a crude estimation of the precipitable water (proportional to the inverse of the moist vertical lapse rate) multiplied by the condensation rate (proportional to the updraft velocity).

The surface depicted in Fig. 5 shows the values of the precipitation index R, calculated near the time of frontal collapse for various values of L and $\Gamma(s_2) - \Gamma(s_1)$. We observe two main trends. The first one, more evident, leads to increasing R for decreasing values of L down to short-wave cutoff. Below this limit, the perturbation is initially decaying, as predicted by the linear solution, and no further relevant nonlinear evolution can develop. This first trend is mainly due to the increase of w with decreasing L. The second trend, less evident but still of some relevance, leads to an increase of R with increasing values of $\Gamma(s_2) - \Gamma(s_1)$, that is, moving from the W1D2 soil moisture distribution toward D1W2. This is due to the decreasing of the global stability $(d + m)$, as already foretold by the previous analysis. At the shorter growing wavelength, R is increased by almost 30% (from 0.9 to 1.15), going from the less to the more favorable soil moisture distribution. This tendency is much stronger for intermediate wavelengths. The R decay for increasing L is much slower when region 2 is wet. As an example, at $L = 2$, R goes from 0.33 to 0.61, with an increase of about 85%.

Figure 6 shows the results for the final growing rate. We observe that this quantity is increased as we move toward wet soil in region 2, so that this moisture distribution may be considered favorable from this point of view as well. While the linear theory predicts a unimodal distribution for the growing rate, with a uniform decrease down to zero at the short-wave cutoff, its variation with decreasing L is more complex in the cases of soil interaction; a second sharp increase is observed, with a sudden and discontinuous nonlinear cutoff at some L.

4. Conclusions

Using an inviscid semigeostrophic model for the evolution of a meridionally independent baroclinic disturbance in the moist atmosphere, the question has been addressed as to what extent and through which mech-

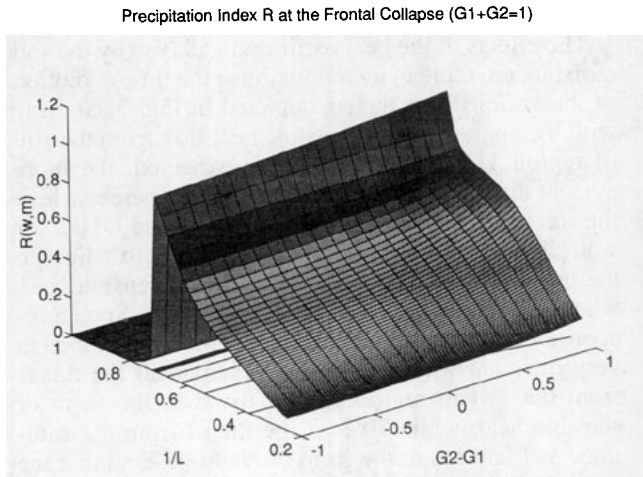

FIG. 5. Precipitation index R as a function of the inverse of the baroclinic half-wavelength ($1/L$), and the difference of saturation between the soil underlying the cold anomaly [$\Gamma(s1)$] and the soil underlying the warm anomaly [$\Gamma(s2)$], with the constraint $\Gamma(s1) + \Gamma(s2) = 1$.

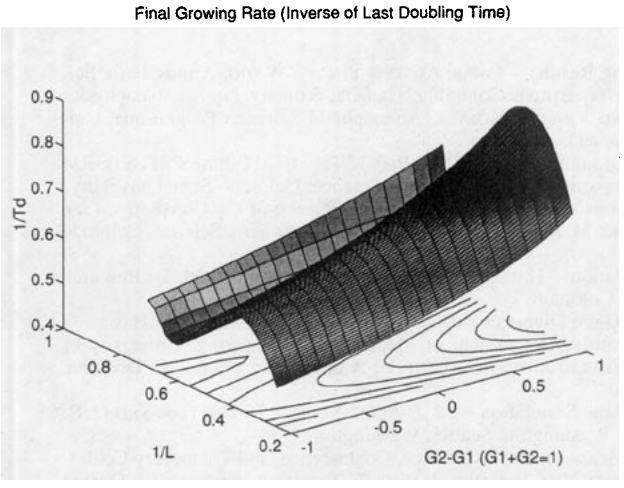

FIG. 6. As in Fig. 5 but for the final growing rate of the baroclinic wave, estimated as the inverse of the last doubling time T_d.

anisms a heterogeneous soil moisture distribution affects the evolution of baroclinic waves and, in particular, the estimate of the potential precipitation. A simplified scheme for the representation of the mass and energy exchange between the soil and the atmospheric boundary layer has been included in order to model the land–atmosphere coupling. Various soil distributions and baroclinic wave characteristics have been tested in order to identify those phase and length configurations of the soil moisture and atmospheric waves that are more favorable. The results of these simulations have been discussed briefly in the previous section, where a complex picture of different feedback mechanisms between the soil moisture and the atmospheric perturbation evolution has been sketched.

Such results may be summarized as follows. The interaction between land and atmosphere has both a local effect and a large-scale effect. The local effect consists of modifying the vertical lapse rates of dry and equivalent potential temperatures. The large-scale effect is realized through the global dynamics of the baroclinic wave and in particular through the rates of mass and energy advection and the strength of the ageostrophic frontal circulation, which themselves strongly depend on the temperature lapse rates. Both effects are found to be substantially dependent on both the local moisture content of the soil and on the large-scale moisture differences, highlighting the feedback character of these effects. In particular, when the warm–moist precipitating anomaly of the baroclinic wave develops on top of a wetter soil, with dryer soil at the cold anomaly, the frontal collapse is reached faster and the estimated precipitation higher (larger updraft velocity and smaller moist stability).

This is just a preliminary step in the study of such a complex problem. Further developments are needed to investigate, for example, the role of the soil moisture distribution in the triggering of the baroclinic instabilities, that is, in the definition of a "land-dependent" initial forcing state of the atmosphere. Strictly connected to this particular issue is the definition of a more realistic radiative scheme, other than the simple radiative initial equilibrium, to be included in the formulation of a less rigid boundary layer parameterization.

Acknowledgments. This work was partially supported by NSF Grant EAR-9120368.

REFERENCES

Chang, J.-T., and P. J. Wetzel, 1991: Effects of spatial variations of soil moisture and vegetation on the evolution of a prestorm environment: A numerical case study. *Mon. Wea. Rev.*, **119,** 1368–1382.

Emanuel, K. A., M. Fantini, and A. J. Thorpe, 1987: Baroclinic instability in an environment of small stability to slantwise moist convection. Part I: Two-dimensional models. *J. Atmos. Sci.*, **44,** 1559–1573.

Fantini, M., 1991: Baroclinic instability and induced air–sea heat exchange. *Tellus,* **43**A, 285–294.

Fast, J. D., and M. D. McCorcle, 1991: The effect of heterogeneous soil moisture on a summer baroclinic circulation in the central United States. *Mon. Wea. Rev.*, **119,** 2140–2167.

Lowry, W. P., 1959: The falling rate phase of evaporative soil moisture loss—A critical evaluation. *Bull. Amer. Meteor. Soc.*, **40,** 605–608.

Ookouchi, Y., M. Segal, R. C. Kessler, and R. A. Pielke, 1984: Evaluation of soil moisture effects on the generation and modification of mesoscale circulations. *Mon. Wea. Rev.*, **112,** 2281–2292.

Segal, M., R. Avissar, M. C. McCumber, and R. A. Pielke, 1988: Evaluation of vegetation effects on the generation and modification of mesoscale circulations. *J. Atmos. Sci.*, **45,** 2268–2291.